

## Excitation and direct imaging of surface plasmon polariton modes in a two-dimensional grating

Kevin A. Tetz,<sup>a)</sup> Rostislav Rokitski, Maziar Nezhad, and Yeshaiahu Fainman  
*Department of Electrical and Computer Engineering, University of California, San Diego,  
 California 92093*

(Received 16 July 2004; accepted 21 January 2005; published online 8 March 2005)

We describe the simultaneous excitation and direct far-field imaging of the scattering from surface plasmon polariton modes in a two-dimensional metallic hole array grating. Conditions for the coupling and imaging are discussed, where the coupling is shown to be consistent with both measured and calculated dispersion relations. Excitation is accomplished at several different wavelengths (from 1.31 to 1.57  $\mu\text{m}$ ), incidence angles, and grating periods, enabling the observation of a number of distinct modes with various in-plane wave vectors. © 2005 American Institute of Physics. [DOI: 10.1063/1.1883334]

Surface plasmon polaritons (SPPs) have been extensively studied for several decades.<sup>1</sup> There has been a variety of recent work that, among other things, has explored their potential for building various integrated optical devices.<sup>2,3</sup> The intrinsic mode confinement, due to their surface nature, may have potential advantages for building subdiffraction limited waveguides<sup>4</sup> and in facilitating full three-dimensional optical confinement.<sup>5,6</sup> Further interest has been sparked by the observation that SPP waves can enhance the transmittance through optically thick metallic films with subwavelength features.<sup>7-10</sup> The radiated diffraction pattern can also be controlled by the excited SPPs.<sup>11</sup> There are a number of fundamental issues still being addressed in the attempt to make practical SPP optical elements. Because of the surface nature of the SPP wave, it is not typically possible to observe them directly in the far field. Imaging can be accomplished in a variety of ways including near-field probing,<sup>12-14</sup> fluorescence imaging,<sup>15</sup> light scattering from surface roughness,<sup>16,17</sup> and, more recently, Fourier domain observations of scattering in a grating array.<sup>18</sup> While it is well known that a grating can overcome a momentum mismatch for the excitation of SPPs,<sup>1</sup> they have not been used to enable imaging in the far field from partially scattered SPPs with an appreciable propagation length. One plausible explanation is that much of the work described thus far has been done at visible wavelengths (or  $\lambda < \sim 1 \mu\text{m}$ ). The damping of propagating SPP waves decreases dramatically from the visible portion of the spectrum into the near infrared,<sup>1,2,19</sup> leading to several advantageous properties of SPPs at these wavelengths. In this letter, we describe techniques for the simultaneous excitation and imaging of various SPP modes in a two-dimensional (2D) periodic hole array, and show that these features are consistent with the dispersion relation for SPPs on a periodically modulated surface. In addition, we directly demonstrate coupling to a number of distinct modes in 2D lattices at near-infrared (from 1.31 to 1.57  $\mu\text{m}$ ) wavelengths.

Samples were prepared as follows: Quartz glass substrates were first cleaned, and a thin ( $\sim 2 \text{ nm}$ ) Ni adhesion layer was deposited followed by approximately 35 nm of gold. Inclusion of this adhesion layer affects the SPP modes

at this interface (stronger damping, in particular), modifying those that would otherwise exist at the glass-gold interface;<sup>20,21</sup> we will therefore refer, instead, to a glass-metal (GM) interface. A mask was then formed using electron-beam direct writing, and the desired pattern—circular holes, of approximately 400 nm diameter, in square arrays of 80  $\mu\text{m}$  with a hole period  $a$  varying from 1.0 to 2.6  $\mu\text{m}$  in increments of 0.1  $\mu\text{m}$ —was then transferred to the metal film via wet chemical etching. Samples were characterized optically using two illumination procedures: (1) A collimated broadband light source was used for measurements of the zero-order transmittance as a function of wavelength and incidence angle (referred to hereafter as “spectral measurements”), and (2) a focused laser beam of varying frequency was used to excite and image the grating scattered leakage from propagating SPPs. For the spectral measurements, illumination from the lamp is collimated, polarized, and the central portion of the array is imaged onto the input slit of a monochromator, which scans a fixed spectral range from 1000 nm to 1700 nm. An InGaAs focal plane array was used for imaging and alignment. The sample was first aligned normal to the beam axis, while the polar angle (i.e., angle of incidence) was increased to 20° in increments of 2°. The measured zero-order transverse magnetic (TM) (i.e., electric field in the plane of incidence) transmittance is shown in Fig. 1 in linear gray scale as a function of frequency and incident wave vector. These data and measurement are similar to that shown in Ghaemi *et al.*,<sup>8</sup> and Barnes *et al.*,<sup>10</sup> though it is important to note that the films measured here are much thinner. The measured transmittance for a number of samples with various periods has been normalized by the hole area per unit cell, and combined to give a full perspective on the SPP excitation conditions for our entire sample and characterization space. The spectra are dominated by transmittance dips at the various SPP excitation conditions, which appear as the set of dark stripes. These major features of the dispersion map are well described by the relation:<sup>1,7,8</sup>  $k_{\text{SPP}} = k_{\parallel} \pm iG_x \pm jG_y$ , where  $k_{\text{SPP}}$  is the SPP wave vector,  $k_{\parallel}$  is the in-plane component of the incident electromagnetic wave vector, and  $G_x$  and  $G_y$  are the reciprocal lattice vectors in the  $x$  and  $y$  directions, respectively. Dispersion curves are calculated for the air-metal (AM) and GM interfaces, shown in Fig. 1 ( $+ak_{\parallel}/2\pi$  direction), and follow

<sup>a)</sup>Electronic mail: ktetz@ece.ucsd.edu

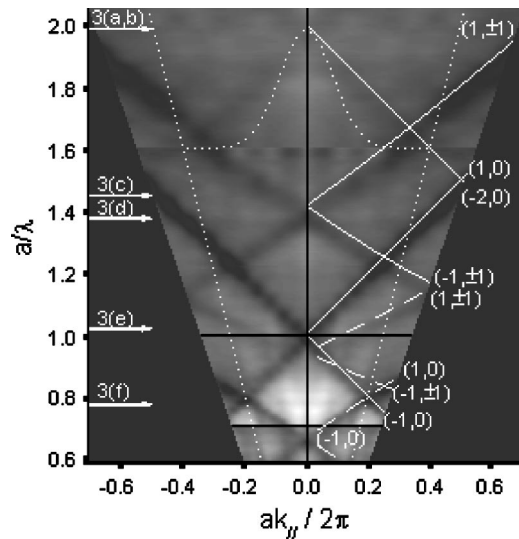


FIG. 1. Spectral measurements of TM polarized zero-order transmittance (transverse electric data not shown) for cubic arrays of holes in a thin gold film on a glass substrate. Data from several arrays with different periods  $a$  have been combined for these composite intensity images, where the stitching frequencies appear as horizontal black lines (identical data are also replicated for  $ak_y/2\pi < 0$  for viewing). The transmittance has been normalized by the hole area per unit cell, and the intensity range is from 0 (dark) to 1.1 (light). On the right half ( $+ak_y/2\pi$ ), the calculated SPP dispersion curves for AM (-) and GM (-) interfaces are seen as white lines. Arrows on the left indicate the position on normalized frequency axis where single frequency laser measurements (shown in Fig. 3) occur. Also sketched (dotted white lines) is the angular spectrum and relative intensity for the incident beam of Fig. 3, with a NA of 0.25.

the SPP features for all of the data on the normalized frequency scale quite well. Only those modes that are efficiently excited—and therefore appear as spectral features in these data—are shown [i.e.,  $(i, j) = (0, 1)$  type modes and higher-order GM modes have been omitted]. Specifically, we see that the  $(\pm 1, 0)$  SPP modes of the AM and GM interfaces, as well as the  $(\pm 1, \pm 1)$  of the AM interface appear under these conditions. The relatively weak coupling to the GM interface (compared to the AM side) is likely due to the damping from the nickel adhesion layer, where the  $(\pm 1, 0)$  order is observable in the spectrum but the  $(\pm 1, \pm 1)$  trait appears barely discernible. More rigorous methods<sup>18,22,23</sup> are required to theoretically determine the relative strength of the coupling as well as the absolute spectral shape of the various bound and propagating diffraction orders. Also sketched in Fig. 1 is the angular spectrum for the excitation with the single frequency sources, defined by the Gaussian spectrum of the incident laser beam, and the angular bandwidth of the MO.

For the laser illumination, a microscope objective (MO) with relatively low numerical aperture (NA)=0.25 was used to focus the beam to a spot of  $\sim 10 \mu\text{m}$  on the sample, and another MO (NA=0.25) and lens ( $f=125 \text{ mm}$ ) pair was used to image the array under observation. In addition, a polarizer-analyzer pair is used to control the polarization state of the excitation field and the field in the image plane, as described in detail shortly. This apparatus is similar to that illustrated in Altewischer *et al.*,<sup>18</sup> except that the detector array is at an image plane rather than a Fourier transform plane, and is sketched in Fig. 2.

Scattering from SPPs observed under various conditions is shown in Fig. 3 (with each period to wavelength ratio

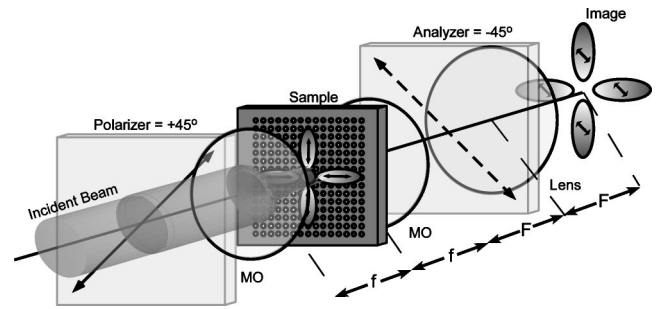


FIG. 2. Schematic of SPP imaging configuration. Illumination on a given sample is from a focused laser (with a microscope objective, MO). The resulting SPP mode is then imaged on to an InGaAs camera array via a  $4F$  imaging system (MO and Lens). For the case shown, the incident polarization at  $45^\circ$  is decomposed into two orthogonal components which excite  $(1,0)$ -type SPP modes which propagate along the grating surface and reradiate in both the forward and backward directions with the illustrated polarization. The radiation is then polarized at  $-45^\circ$  to obtain the field in the image plane.

labeled as an arrow at the corresponding frequency in Fig. 1). At these positions, when the phase matching conditions are satisfied, an exponentially decaying SPP mode is excited in a direction dictated by the resultant SPP  $k$  vector. This is seen as crossed lobes extending out from the center of the illumination spot. In Figs. 3(a) and 3(b), the excitation and imaging conditions are identical; however, in Fig. 3(a), the polarizer and analyzer are parallel at  $45^\circ$  [the  $(1, 1)$  direction]. In Fig. 3(b), the analyzer is instead rotated to  $-45^\circ$ , which effectively nulls the uncoupled, zero-order transmitted beam.<sup>18</sup> Note that Figs. 3(a) and 3(b) correspond to excitation of  $(\pm 2, 0)$ ,  $(0, \pm 2)$  modes, and, although weak, are readily observable. This is in contrast to the spectral data, where the excitation of these modes is below the signal-to-noise ratio for our setup (Fig. 1). Figures 3(c)–3(f) each show images for other experimental conditions: Figs. 3(c) and 3(d) correspond to excitation of  $(\pm 1, \pm 1)$ -type modes at different frequencies (in different hole arrays); Fig. 3(e) shows  $(\pm 1, 0)$ ,  $(0, \pm 1)$  excitation; Fig. 3(f) shows an image when there is no excitation—the intersection of the angular intensity profile and the period-to-wavelength ratio do not lead to excitation of any mode with appreciable efficiency. Note also

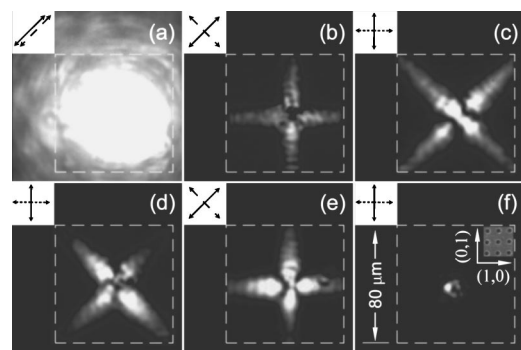


FIG. 3. SPPs observed in various hole arrays. Inset is the relative polarizer (solid) and analyzer (dashed) orientation for each image. Intensity scales for (a) and (b) are identical, while (c)–(f) have been adjusted to observe the full SPP extent. Also inset in (f) is a distance bar valid for all optical images, and a scanning electron microscope image that shows a representative array and the hole orientation relative to the optical images. The respective hole period  $a$  and free-space laser wavelength  $\lambda$  are (in  $\mu\text{m}$ ): (a) and (b)  $a=2.60$ ,  $\lambda=1.31$ ; (c)  $a=2.20$ ,  $\lambda=1.52$ ; (d)  $a=1.80$ ,  $\lambda=1.31$ ; (e)  $a=1.60$ ,  $\lambda=1.57$ ; and (f)  $a=2.20$ ,  $\lambda=1.52$ .

that Fig. 3(f) is at a position of maximum transmittance at zero-polar angle, and we clearly see that excitation of propagating SPPs do not enhance that transmittance for our thin films. The SPPs in all cases can only be observed to propagate to the end of the grating, although they assuredly continue on the unmodulated surface.<sup>13,14</sup>

Of particular interest is the SPP propagation length, which, for this case of a grating-modulated surface, is dependent upon both the radiative decay as well as the material damping.<sup>1</sup> The radiative decay of the SPPs must be small enough to observe the spreading of the field over these relatively large distances (several tens of  $\mu\text{m}$ ). For a wavelength of  $1.31\ \mu\text{m}$ , we measure a  $1/e$  decay length of  $22\pm 3$  and  $15\pm 2\ \mu\text{m}$  for the  $(+2, 0)$  and  $(\pm 1, \pm 1)$  modes, respectively (by exciting near the edge of the array, and fitting an exponential curve to a Gaussian fit of the image cross sections averaged over all four directions). Similarly, the  $(\pm 1, \pm 1)$  mode at  $1.52\ \mu\text{m}$  decays in  $26\pm 3\ \mu\text{m}$ , while the  $(\pm 1, 0)$  mode at  $1.57\ \mu\text{m}$  propagates  $14\pm 3\ \mu\text{m}$ . These data may be compared to the estimated decay value for an unperforated infinite AM interface of  $140\ \mu\text{m}$  (at  $1.31\ \mu\text{m}$ ) or  $200\ \mu\text{m}$  (at  $\sim 1.55\ \mu\text{m}$ )—or, perhaps more appropriately, with the anti-symmetric SPP mode of a finite thickness gold film<sup>24</sup> which predicts 23 and  $32\ \mu\text{m}$ , respectively, for the same wavelengths. These values are only marginally less than the  $40\ \mu\text{m}$  seen for a planar gold surface<sup>17</sup> at a  $0.8\ \mu\text{m}$  wavelength despite the relatively strong radiative damping.

In conclusion, we have demonstrated the coupling to SPP modes in a cubic array of holes and the direct observation of leakage radiation from such arrays. A wide variety of propagating waves, with different frequencies and in-plane wave vectors can be excited and observed for various sample geometries and under variable excitation conditions. Such techniques may prove useful for investigating the properties of SPP waves for a variety of applications and in interfacing with various nanoplasmonic devices.

The authors would like to thank Professor H. H. Wieder and Dr. Uriel Levy for helpful discussions. This work is partially funded by the NSF, AFOSR, and DARPA.

- <sup>1</sup>H. Raether, *Surface Plasmons on Smooth and Rough Surfaces and on Gratings* (Springer, Berlin, 1988).
- <sup>2</sup>W. L. Barnes, A. Dereux, and T. W. Ebbesen, *Nature (London)* **424**, 824 (2003).
- <sup>3</sup>H. Ditlbacher, J. R. Krenn, G. Schider, A. Leitner, and F. R. Aussenegg, *Appl. Phys. Lett.* **81**, 1762 (2002).
- <sup>4</sup>S. A. Maier, M. L. Brongersma, P. G. Kik, S. Meltzer, A. A. G. Requicha, and H. A. Atwater, *Adv. Mater. (Weinheim, Ger.)* **13**, 1501 (2001).
- <sup>5</sup>W. L. Barnes, S. C. Kitson, T. W. Preist, and J. R. Sambles, *J. Opt. Soc. Am. A* **14**, 1654 (1997).
- <sup>6</sup>W. L. Barnes, T. W. Preist, S. C. Kitson, and J. R. Sambles, *Phys. Rev. B* **54**, 6227 (1996).
- <sup>7</sup>T. W. Ebbesen, H. J. Lezec, H. F. Ghaemi, T. Thio, and P. A. Wolff, *Nature (London)* **391**, 667 (1998).
- <sup>8</sup>H. F. Ghaemi, T. Thio, D. E. Grupp, T. W. Ebbesen, and H. J. Lezec, *Phys. Rev. B* **58**, 6779 (1998).
- <sup>9</sup>L. Martin-Moreno, F. J. Garcia-Vidal, H. J. Lezec, K. M. Pellerin, T. Thio, J. B. Pendry, and T. W. Ebbesen, *Phys. Rev. Lett.* **86**, 1114 (2001).
- <sup>10</sup>W. L. Barnes, W. A. Murray, J. Dintinger, E. Devaux, and T. W. Ebbesen, *Phys. Rev. Lett.* **92**, 107401 (2004).
- <sup>11</sup>H. J. Lezec, A. Degiron, E. Devaux, R. A. Linke, L. Martin-Moreno, F. J. Garcia-Vidal, and T. W. Ebbesen, *Science* **297**, 820 (2002).
- <sup>12</sup>S. Kawata, *Topics in Applied Physics* (Springer, Berlin, 2001), Vol. 81.
- <sup>13</sup>D. S. Kim, S. C. Hohng, V. Malyarchuk, Y. C. Yoon, Y. H. Ahn, K. J. Yee, J. W. Park, J. Kim, Q. H. Park, and C. Lienau, *Phys. Rev. Lett.* **91**, 143901 (2003).
- <sup>14</sup>E. Devaux, T. W. Ebbesen, J. C. Weeber, and A. Dereux, *Appl. Phys. Lett.* **83**, 4936 (2003).
- <sup>15</sup>H. Ditlbacher, J. R. Krenn, N. Felidj, B. Lamprecht, G. Schider, M. Salerno, A. Leitner, and F. R. Aussenegg, *Appl. Phys. Lett.* **80**, 404 (2002).
- <sup>16</sup>J. R. Krenn and J. C. Weeber, *Philos. Trans. R. Soc. London, Ser. A* **362**, 739 (2004).
- <sup>17</sup>B. Lamprecht, J. R. Krenn, G. Schider, H. Ditlbacher, M. Salerno, N. Felidj, A. Leitner, F. R. Aussenegg, and J. C. Weeber, *Appl. Phys. Lett.* **79**, 51 (2001).
- <sup>18</sup>E. Altewischer, M. P. van Exter, and J. P. Woerdman, *J. Opt. Soc. Am. B* **20**, 1927 (2003).
- <sup>19</sup>T. Goto, Y. Katagiri, H. Fukuda, H. Shinjima, Y. Nakano, I. Kobayashi, and Y. Mitsuoka, *Appl. Phys. Lett.* **84**, 852 (2004).
- <sup>20</sup>D. E. Grupp, H. J. Lezec, T. W. Ebbesen, K. M. Pellerin, and T. Thio, *Appl. Phys. Lett.* **77**, 1569 (2000).
- <sup>21</sup>C. Genet, M. P. van Exter, and J. P. Woerdman, *Opt. Commun.* **225**, 331 (2003).
- <sup>22</sup>M. Sarrazin, J. P. Vigneron, and J. M. Vigoureux, *Phys. Rev. B* **67**, 085415 (2003).
- <sup>23</sup>B. K. Minhas, W. Fan, K. Agi, S. R. J. Brueck, and K. J. Malloy, *J. Opt. Soc. Am. A* **19**, 1352 (2002).
- <sup>24</sup>J. J. Burke, G. I. Stegeman, and T. Tamir, *Phys. Rev. B* **33**, 5186 (1986).